Dalton Transactions

RSC Publishing

PAPER

View Article Online
View Journal | View Issue

Cite this: *Dalton Trans.*, 2013, **42**, 4153

C–N coupling in the gas-phase reactions of ammonia and $[M(CH)]^+$ (M = Ni, Pd, Pt): a combined experimental/computational exercise

Robert Kretschmer,[a,b] Maria Schlangen[a] and Helmut Schwarz*[a,c]

Received 30th October 2012,
Accepted 11th January 2013

DOI: 10.1039/c3dt32596b

www.rsc.org/dalton

Electrospray ionization (ESI) of methanolic solutions of monomeric nickel(II) acetate, $[Ni(CH_3COO)_2]$, and tetrameric platinum(II) acetate, $[Pt_4(CH_3COO)_8]$, leads to the formation of the corresponding methylidyne complexes $[M(CH)]^+$ (M = Ni, Pt), which react with ammonia under C–N coupling. While the product couples $M/[CH_4N]^+$ and $[M(CH_2N)]^+/H_2$ are observed for both metals, hydrogen-atom expulsion to generate $[M(CHNH_2)]^+/H$ is only observed in the case of the nickel-containing system, and the proton transfer leading to $M/[NH_4]^+$ is limited to platinum. Attempts to conduct related experiments with $[Pd(CH)]^+/NH_3$ failed. The mechanisms that explain the experimentally observed reaction channels have been investigated computationally using the B3LYP functional for all metals of the nickel group (M = Ni, Pd, Pt). In line with labeling experiments using the reaction pairs $[M(CD)]^+/NH_3$ and $[M(CH)]^+/ND_3$ (M = Ni, Pt), two different mechanistic scenarios of the dehydrogenation process are operative for the Ni and Pt systems, respectively.

Introduction

The formation of carbon–nitrogen bonds constitutes an important step in the preparation of several products ranging from chemical feedstocks to pharmaceuticals, and over the last few decades, intensive research has been devoted to this topic.[1] The use of ammonia as an inexpensive reagent for C–N coupling reactions is highly desired.[2] Ammonia is consumed on a large scale in industry, and C–N bond coupling reactions are *e.g.* accomplished in the synthesis of urea and in the Degussa process; in the latter, HCN is generated from CH_4 and NH_3 at high temperatures. However, the specific, metal-mediated formation of nitrogen-containing molecules generated directly from NH_3 in homogeneous catalytic reactions under ambient conditions is still rather limited due to the unwanted deactivation of the catalyst by the formation of Werner amine complexes. The improvement of existing and the development of new catalysts can ideally be achieved based on the knowledge of the intrinsic properties of the active metal center and of the underlying reaction mechanism, derived at a molecular level.

One way to gain such insight is studying model systems in the gas phase. Mass-spectrometry-based experiments[3] have for example aided in the identification of CH_2NH as a crucial intermediate in the Degussa process,[4] and its existence has been confirmed later by *in situ* photoionization experiments.[5] In the gas-phase model of the $[Pt]^+$-mediated coupling of ammonia and methane,[4a,6] the generation of $[Pt(CH_2)]^+$ from $[Pt]^+$ and methane constitutes the first step (eqn (1)).

$$[Pt]^+ + CH_4 \rightarrow [Pt(CH_2)]^+ + H_2 \quad (1)$$

$[Pt(CH_2)]^+$ can then react with NH_3 to afford three different product couples (eqn (2)–(4)):[4a,6]

$$[Pt(CH_2)]^+ + NH_3 \rightarrow \begin{cases} [CH_2NH_2]^+ + PtH & 70\% \quad (2) \\ [Pt(CHNH_2)]^+ + H_2 & 25\% \quad (3) \\ [NH_4]^+ + PtCH & 5\% \quad (4) \end{cases}$$

Also $[PtC]^+$ and $[Pt(CH)]^+$ bring about C–N coupling in the reaction with ammonia;[6b,7] the complex $[Pt(CH)]^+$ can be generated by electrospray ionization of the tetrameric platinum(II) acetate, $[Pt_4(CH_3COO)_8]$, dissolved in methanol[7] or by collision-induced dissociation of $[Pt(CH_2)]^+$.[6b] As demonstrated earlier,[4,6–8] the nature of the metal center crucially influences reaction efficiencies, branching ratios, and the generated product species in C–N coupling reactions.[9] In order to uncover similarities and differences, and to explore trends within group 10 of the periodic table, we envisaged expanding the investigation to the $[Ni(CH)]^+/NH_3$ and $[Pd(CH)]^+/NH_3$

[a]*Technische Universität Berlin, Institut für Chemie, Straße des 17.Juni 115, 10623 Berlin, Germany. E-mail: Helmut.Schwarz@mail.chem.tu-berlin.de; Fax: +49 30 314 21102; Tel: +49 30 314 23483*
[b]*University of California San Diego, Department of Chemistry and Biochemistry, La Jolla, CA 92093-0343, USA*
[c]*King Abdulaziz University, Faculty of Science, Department of Chemistry, P. O. Box 80203, 21589 Jeddah, Saudi Arabia. E-mail: HSchwarz@kau.edu.sa*

couples. The focus is particularly on the capability of C–N bond formation, and the mass-spectrometric experiments are complemented by kinetic and labeling studies as well as by computational investigation. However, while $[Pt(CH)]^+$ and $[Ni(CH)]^+$ complexes can easily be generated by electrospray ionization, $[Pd(CH)]^+$ is not accessible by this method; thus, the potential reactivity of this ion can, for the time being, only be probed by computational studies.

Experimental

Reagents

Acetic acid, acetic acid-D_4, nickel(II) acetate, nickel(II) carbonate hydrate, palladium(II) acetate, silver acetate and methanol were purchased from Sigma-Aldrich and were used without further purification. $[Pt_4(CH_3COO)_8]$ was prepared from platinum(II) chloride and silver acetate in acetic acid, as described in detail previously.[10] $[Pt_4(CD_3COO)_8]$ was synthesized analogously by using $[Ag(CH_3COO)]$ and CD_3COOD in a molar ratio of about 1 : 100. $[Ni(CD_3COO)_2]$ was prepared by treating basic nickel(II) carbonate hydrate with CD_3COOD. Dry ammonia (99.98%) was obtained from Air Liquide and ND_3 (99.0 atom-% D) was purchased from Sigma-Aldrich.

Mass spectrometry and ion/molecule reactions

The experiments were performed with a VG Bio-Q mass spectrometer of QHQ configuration (Q: quadrupole; H: hexapole) equipped with an electrospray-ionization (ESI) source, as described in detail elsewhere.[11] Millimolar solutions of $[Ni(CH_3COO)_2]$ and $[Pt_4(CH_3COO)_8]$ in pure methanol were used for the production of $[M(CH)]^+$.[7] The solutions were introduced through a fused-silica capillary to the ESI source *via* a syringe pump (*ca.* 4 μL min^{-1}) in order to produce the metal-complex cations. Nitrogen was used as a nebulizing and drying gas at a source temperature of 80 °C. Maximum yields of the desired complexes were achieved by adjusting the cone voltage (U_c); U_c determines the degree of collisional activation of the incident ions in the transfer from the ESI source to the mass spectrometer.[11] The identity of the ions was confirmed by comparison with the expected isotope patterns.[12] The ion/molecule reactions of the complexes with ammonia were probed at a collisional energy (E_{lab}) set to nominally 0 eV, which in conjunction with the *ca.* 0.4 eV kinetic energy width of the parent ion at half peak height allows the investigation of quasi-thermal reactions, as demonstrated previously.[13] Finally, all given branching ratios were determined by extrapolating the branching ratios at different pressures of ammonia to $p(NH_3) = 0$.

DFT calculations

In the computational studies we employed the Gaussian 09 program package[14] using the B3LYP functional.[15] For C, H, and N we used the triple-ξ plus polarization (TZVP) basis sets of Ahlrichs and co-workers.[16] For Ni, Pd, and Pt, the Stuttgart–Dresden scalar relativistic pseudopotentials in conjunction with the corresponding basis sets were employed.[17] The validity of this protocol has already been proven by comparing the experimental and theoretical value of $BDE(Pt^+–CH)$.[18] For $[Ni(CH)]^+$ the calculated BDE value of 311.0 kJ mol^{-1} is within the uncertainty of the experimental value (301.0 ± 11.6 kJ mol^{-1});[19] $BDE(Pd^+–CH)$ has, to the best of our knowledge, not been reported in the literature. All energies (given in kJ mol^{-1}) are corrected for (unscaled) zero-point vibrational energy contributions.

Results and discussion

Experimental results

Fig. 1 shows the mass spectra for the thermal reactions of mass-selected $[Ni(CH)]^+$ and $[Pt(CH)]^+$ with ammonia, with the reaction products given in eqn (5)–(10).

$$[Ni(CH)]^+ + NH_3 \rightarrow [CH_2NH_2]^+ + Ni \quad 37\% \quad (5)$$
$$\rightarrow [Ni,C,H_2,N]^+ + H_2 \quad 18\% \quad (6)$$
$$\rightarrow [Ni(CHNH_2)]^+ + H \quad 45\% \quad (7)$$

$$[Pt(CH)]^+ + NH_3 \rightarrow [CH_2NH_2]^+ + Pt \quad 51\% \quad (8)$$
$$\rightarrow [Pt,C,H_2,N]^+ + H_2 \quad 35\% \quad (9)$$
$$\rightarrow [NH_4]^+ + PtC \quad 14\% \quad (10)$$

In accordance with previous results,[7] three product couples are observed when $[Pt(CH)]^+$ is reacted with ammonia. The

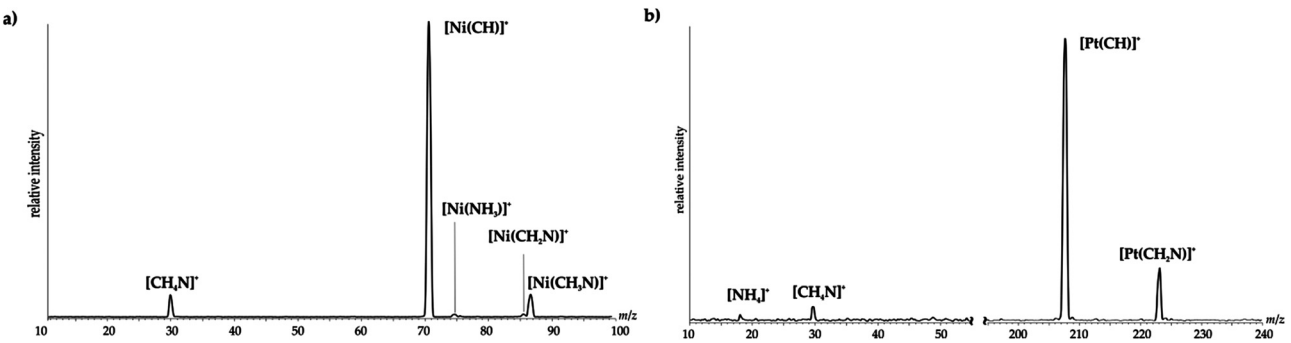

Fig. 1 Mass spectra resulting from the ion/molecule reactions of mass-selected (a) $[Ni(CH)]^+$ and (b) $[Pt(CH)]^+$ with ammonia at a pressure of 4.0×10^{-4} mbar.

main reaction channel corresponds to the elimination of neutral Pt (eqn (8)) concomitant with the formation of cationic $[CH_4N]^+$ (*m*/*z* 30). The latter species features also prominently in the mass spectra of amines,[20] and the methane-iminium ion $[CH_2NH_2]^+$ was found to be the most stable of all conceivable isomers.[21] Moreover, dehydrogenation to produce $[Pt,C,H_2,N]^+$ (eqn (9)) and proton transfer to ammonia to generate $[NH_4]^+$ (eqn (10)) are observed. The formation of $[Pt,C,H_2,N]^+$ also takes place in the reaction of $[PtC]^+$ with NH_3, and $[NH_4]^+$ as well as $[CH_2NH_2]^+$ are known as product ions for the $[Pt(CH_2)]^+/NH_3$ couple.[6] The reaction of $[Ni(CH)]^+$ with ammonia is slightly less efficient (k_{rel} = 70% relative to the $[Pt(CH)]^+/NH_3$ system). While the product ions $[CH_2NH_2]^+$ and $[M,C,H_2,N]^+$ are also observed for M = Ni (eqn (5) and (6)), the formation of $[NH_4]^+$ is not observed at the detection limit. However, an additional reaction channel was identified that corresponds to the generation of $[Ni,C,H_3,N]^+$ concomitant with the release of a hydrogen atom; the structural assignment of $[Ni(CHNH_2)]^+$ for the product ion (eqn (7)) is based on the theoretical results (see below). Additionally, $[Ni(NH_3)]^+$ has been observed, and it must have been formed in a secondary reaction (eqn (11)); this assignment is based on the fact that the direct formation of this ion *via* a ligand exchange $[Ni(CH)]^+ + NH_3 \rightarrow [Ni(NH_3)]^+ + CH$ is calculated to be endothermic by 63 kJ mol^{-1}; thus, this process is not accessible under thermal or quasi-thermal conditions.[19,22]

$$[Ni(CH)]^+ + 2NH_3 \rightarrow [Ni(NH_3)]^+ + [CH_4N] \quad (11)$$

The assignments of the reaction channels given in eqn (5)–(11) are in keeping with labeling experiments employing the couples $[M(CD)]^+/NH_3$ and $[M(CH)]^+/ND_3$ (M = Ni, Pt). These experiments provide further insight into the origin of the neutral products H_2 and H of the reactions 6, 7, and 9. The exclusive deuterium and hydrogen atom losses according to eqn (7a) and (7b), respectively, indicate a specific N–H bond activation of ammonia. In contrast, for both M = Ni and Pt, hydrogen/deuterium scrambling processes and/or coexisting reaction mechanisms are operative in the dehydrogenation according to eqn (6a/9a) and (6b/9b). While for the $[Ni(CH)]^+/ND_3$ couple the loss of D_2 (eqn (6a)) is preferred compared to that of HD elimination (eqn (9a)), the opposite is observed for $[Pt(CH)]^+/ND_3$; analogous results are obtained for the corresponding $[M(CD)]^+/NH_3$ pairs.[23] In the case of random D_2/HD or H_2/HD losses from the couples $[M(CH)]^+/ND_3$ or $[M(CH)]^+/ND_3$, respectively, 50 : 50 ratios would have been expected; consequently, different reaction mechanisms must apply for the two metals.

$$[Ni(CH)]^+ + ND_3 \rightarrow [Ni(CHND_2)]^+ + D \quad (7a)$$

$$[Ni(CD)]^+ + NH_3 \rightarrow [Ni(CDNH_2)]^+ + H \quad (7b)$$

$$[M(CH)]^+ + ND_3 \rightarrow \begin{cases} [M,C,H,D,N]^+ + D_2 \\ [M,C,D_2,N]^+ + HD \end{cases} \quad (6a/9a)$$

$$[M(CD)]^+ + NH_3 \rightarrow \begin{cases} [M,C,H,D,N]^+ + H_2 \\ [M,C,H_2,N]^+ + HD \end{cases} \quad (6b/9b)$$

Computational results

DFT calculations were performed to obtain mechanistic insights concerning the different pathways observed in the reactions of $[M(CH)]^+$ (M = Ni, Pt) with ammonia; the analogous reaction pathways have also been calculated for M = Pd. For $[M(CH)]^+$ two isomers were located on the potential-energy surfaces (PESs), *i.e.* the carbyne $[M(CH)]^+$ as well as the hydrido carbide $[HMC]^+$; however, the latter isomer is much higher in energy for all three metals (by 421 kJ mol^{-1}, 160 kJ mol^{-1}, and 90 kJ mol^{-1} for M = Ni, Pd, and Pt, respectively) and thus does not play a role in thermal reactions. For all three metals, the singlet state of $[M(CH)]^+$ corresponds to the electronic ground state, and the singlet–triplet splitting increases in the series Ni, Pd, Pt ($\Delta E_{sing-trip}$ = 14.9, 53.1, and 162.3 kJ mol^{-1} for M = Ni, Pd, and Pt, respectively).

Fig. 2 summarizes the PESs associated with the formations of the $M/[CH_2NH_2]^+$ pairs for M = Ni, Pd, Pt; the relative energies are given in Table 1. Starting from $[M(CH)]^+$, ammonia can coordinate either to the metal center leading to the Werner complex **1** or to the carbon center to give **2** directly under the formation of a C–N bond. **1** and **2** can isomerize *via* $\mathbf{TS_{1/2}}$, which is located energetically below the entrance channel for all three metals. Starting from complex **2**, a hydrogen shift from nitrogen to carbon occurs to produce a CH_2NH_2 moiety; two different pathways exist: (i) in metal-mediated processes *via* transition structures $\mathbf{TS_{2/3}}$ and $\mathbf{TS_{3/4}}$ or (ii) directly *via* $\mathbf{TS_{2/4}}$ as an *intra*-ligand shift without the participation of the metal center. Despite several efforts, it was not possible to locate $^3\mathbf{TS_{2/3}}$ for M = Ni and $^1\mathbf{TS_{2/4}}$ for M = Pd and Pt. After the formation of the $[M(CH_2NH_2)]^+$ complex **4**, dissociation leads to the observed product couples $M/[CH_2NH_2]^+$. The exothermicity of the whole process increases from platinum to nickel to palladium, reflecting the strong Pt–C bond in $[Pt(CH)]^+$ due to relativistic effects.[24] The charge-reversed, alternative product pairs $[M]^+/CH_2NH_2$ in their ground states are with 162.1 kJ mol^{-1} for Ni, 223.0 kJ mol^{-1} for Pd, and 276.2 kJ mol^{-1} for Pt higher in energy relative to the formation of the ground state neutral metals, respectively, in line with the higher ionization energies of the metals, *i.e.* (IE(Pt) = 868.4 kJ mol^{-1},[25] IE(Pd) = 804.4 kJ mol^{-1},[26] IE(Ni) = 733.7 kJ mol^{-1},[27] compared to IE(CH_2NH_2) = 606.9 kJ mol^{-1}).[21c] However, the $[Ni]^+/CH_2NH_2$ couple in the high spin and low spin states as well as the $^2[Pd]^+/CH_2NH_2$ product pair are located energetically below the entrance channel and should therefore be accessible under thermal conditions; yet, the non-occurrence of these product ions reflects the much more favoured formation of the neutral metal atoms together with $[CH_2NH_2]^+$.

As shown in Fig. 2 and Table 1, a two-state reactivity (TSR) scenario,[28] which is crucial in numerous reactions of cationic nickel complexes in the gas phase,[29] is not necessarily involved

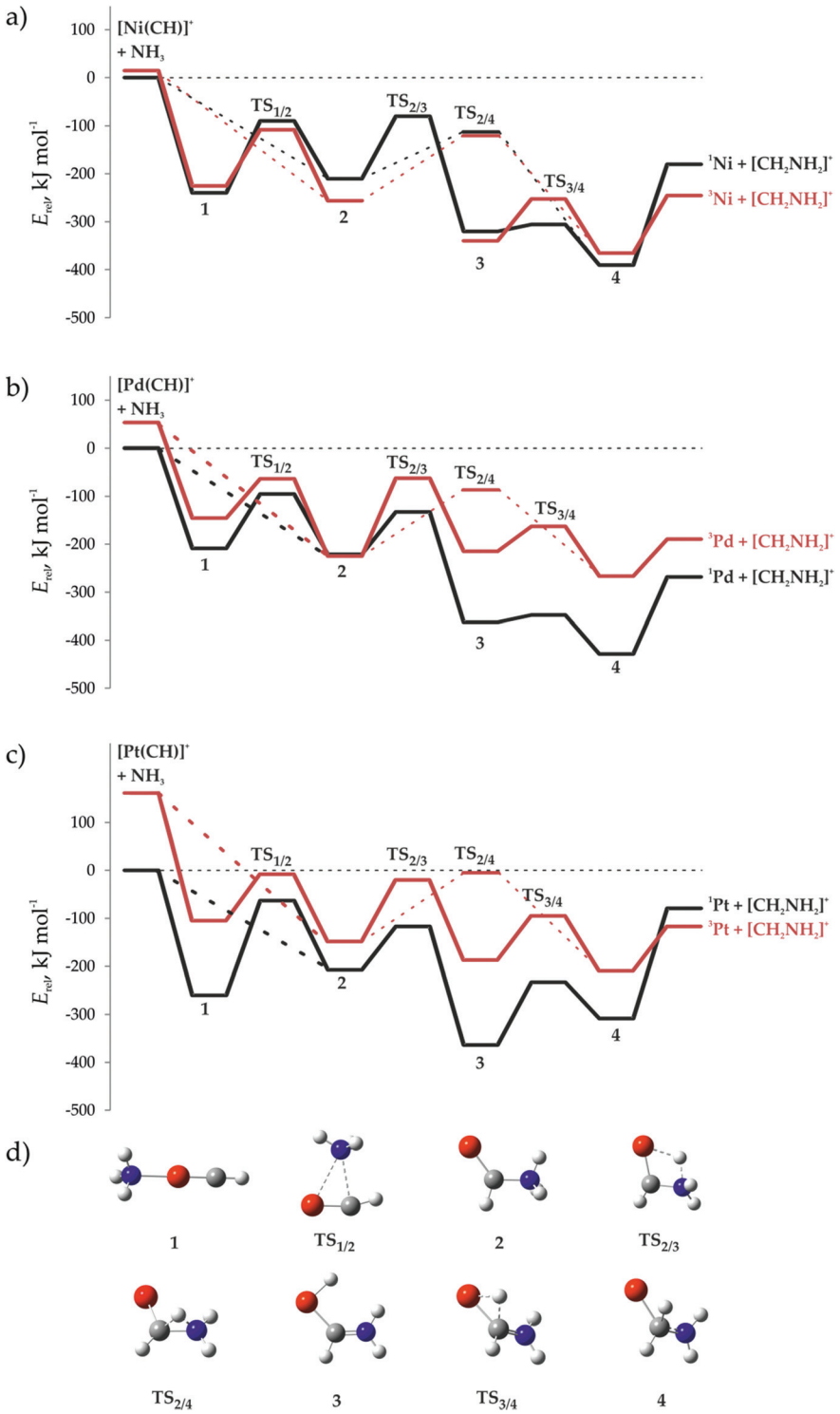

Fig. 2 Schematic potential-energy surfaces for the formations of $M/[CH_2NH_2]^+$ from $[M(CH)]^+/NH_3$ for (a) Ni, (b) Pd, and (c) Pt. The structures of the corresponding minima and transition states are given in (d). The energies are given relative to the singlet ground states of the educts; for details, see Table 1. For the sake of clarity, charges are omitted. C ●, H ●, N ●, metal ●.

in these reactions because all intermediates and transition structures in their low-spin ground state are lower in energy compared to the entrance channel. Thus, the possible involvement of a TSR scenario is largely controlled by the efficiency of the spin–orbit coupling which is the highest for platinum. For the latter system, however, the high spin and low spin surfaces do not cross in the course of the reaction. Here, the triplet state is the ground state only of the exit channel; thus, a spin

Table 1 Relative energies (given in kJ mol^{-1}) of all ground (singlet) and first-excited (triplet) state species shown in Fig. 2

	Ni		Pd		Pt	
	s	t	s	t	s	t
$[M(CH)]^+ + NH_3$	0.0	14.9	0.0	53.1	0.0	162.3
1	−243.6	−229.3	−209.0	−145.6	−260.4	−105.1
$TS_{1/2}$	−93.5	−112.2	−95.3	−63.6	−63.2	−7.9
2	−214.4	−260.5	−221.3	−225.1	−207.8	−148.6
$TS_{2/3}$	−84.2	[a]	−132.9	−62.5	−117.2	−20.0
3	−324.4	−339.9	−362.7	−214.8	−363.8	−187.6
$TS_{3/4}$	−305.7	−252.6	−347.5	−163.0	−233.0	−95.0
$TS_{2/4}$	−120.3	−123.6	[a]	−86.6	[a]	−5.7
4	−394.7	−369.8	−428.0	−277.0	−308.8	−209.7
$M + [CH_2NH_2]^+$	−184.1	−249.5	−268.3	−189.5	−79.2	−117.2
$[M]^+ + CH_2NH_2$	−87.4	−9.0	−45.3	233.7	159.0	236.0
$MC + [NH_4]^+$	63.0	91.8	27.4	33.4	−72.0	56.2

[a] No stable geometry could be obtained.

crossing might take place in the last step of the formation of the products $[CH_2NH_2]^+$ and neutral Pt. With the triplet ground state of neutral Ni, a crossing from the singlet ground state of the educts to the triplet surface would also render the reaction more exothermic for the nickel system. Only neutral Pd possesses a d^{10} singlet ground state, *i.e.* no spin crossing is necessary in this case to form the products in their singlet ground state.

As already mentioned, the ammonium ion $[NH_4]^+$ is only observed in the reactions of the $[Pt(CH)]^+/NH_3$ couple, eqn (10). This is in good agreement with the calculated proton affinities (PAs) of the metal carbides; while PA(NiC) = 915.1 kJ mol^{-1} and PA(PdC) = 879.5 kJ mol^{-1} exceed PA(NH_3) = 852.1 kJ mol^{-1}, platinum carbide possesses a lower proton affinity (PA(PtC) = 780.1 kJ mol^{-1}), and is thus able to act as a Brønsted acid.

Besides the formation of $M/[CH_2NH_2]^+$, we also observe the product ions $[M,C,H_2,N]^+$ (M = Ni, Pt) and $[Ni,C,H_3,N]^+$. The associated reaction pathways have also been investigated by means of DFT calculations; the latter indicate that C–N coupling is involved also in these reactions. A schematic potential-energy surface is shown in Fig. 3 and the corresponding energies are given in Table 2. As demonstrated by Diefenbach *et al.*,[4a] the amino carbene species $[M(CHNH_2)]^+$ corresponds to the most stable isomer of $[M,C,H_3,N]^+$ in the case of platinum; according to our calculations, this holds also true for nickel and palladium. Further, the elimination of a hydrogen atom to generate $[M(CHNH_2)]^+$ proceeds from **3**; the corresponding product ion is not observed experimentally for platinum but only for nickel (reaction 7). In line with this, the M–H bond strength in intermediate **3** increases from nickel to platinum; thus, while the elimination of hydrogen is with 156.1 kJ mol^{-1} exothermic for nickel, it is endothermic for palladium (37.3 kJ mol^{-1}) and platinum (81.2 kJ mol^{-1}), respectively.

Table 3 summarizes some relevant geometric parameters of selected species given in Fig. 2 and 3. The M–C bond lengths in $[M(CH)]^+$ (M = Ni, Pd, Pt) are in good agreement with data obtained from the triple bond radii approach of Pyykkö and co-workers.[30] While this holds also true for **1** and $TS_{1/2}$, the M–C bond in **2** is elongated by 0.1 Å leading to a double bond character.[31] In intermediate **4**, the M–C bond length exceeds the value of the single bond radii approach[31,32] and is best described as a coordinative bond. By comparing the C–N bond in **4** with that in free $[CH_2NH_2]^+$ (1.27 Å) an elongation of 0.1 Å is observed which can be explained by a transfer of electron density from the metal into antibonding orbitals of the ligand.

For the product ion of the dehydrogenation process, one has to consider two isomers $[M(CHNH)]^+$ (**7a**) and $[M(CNH_2)]^+$ (**7b**) which can both be formed starting from intermediate **3** (paths I and II, respectively, Fig. 3). Transition structure $TS_{3/6a}$ of path I possesses a five-membered ring, while $TS_{3/6b}$ of path II corresponds to a planar four-membered ring; accordingly, it is a prototype of a genuine transition structure of a σ-bond metathesis reaction. As discussed in the context of methane activation by transition metal hydrides,[33] the transition structure of this type of reaction is more stable in the low spin state. This holds true for $TS_{3/6b}$ of the Ni and Pd systems and for $TS_{3/6a}$ in the case of palladium which are 10.4 kJ mol^{-1}, 65.9 kJ mol^{-1}, and 55.7 kJ mol^{-1} lower in the corresponding singlet states, respectively; for platinum, we did not succeed in locating $^1TS_{3/6a}$ and a transition structure for either the singlet or triplet states of $TS_{3/6b}$ (see below). With respect to the exothermicities of the respective dehydrogenation processes, the formation of $[M(CHNH)]^+$ (**7a**, path I) is for nickel and palladium energetically favoured by *ca.* 30 kJ mol^{-1}, while for platinum the product ion $[M(CNH_2)]^+$ (**7b**, path II) is more stable.

As mentioned above, for $TS_{3/6a}$ neither on the singlet nor on the triplet surface a transition state could be located for platinum; here, the initial structures instead converge to species formed in a sequence of an oxidative addition (OA)/reductive elimination (RE) process and to a β-hydrogen transfer, respectively, Fig. 4. Similar trends have been reported before for the dehydrogenation of methane by group 10 transition-metal hydrides $[MH]^+$ (M = Ni, Pd, Pt)[34] or in the

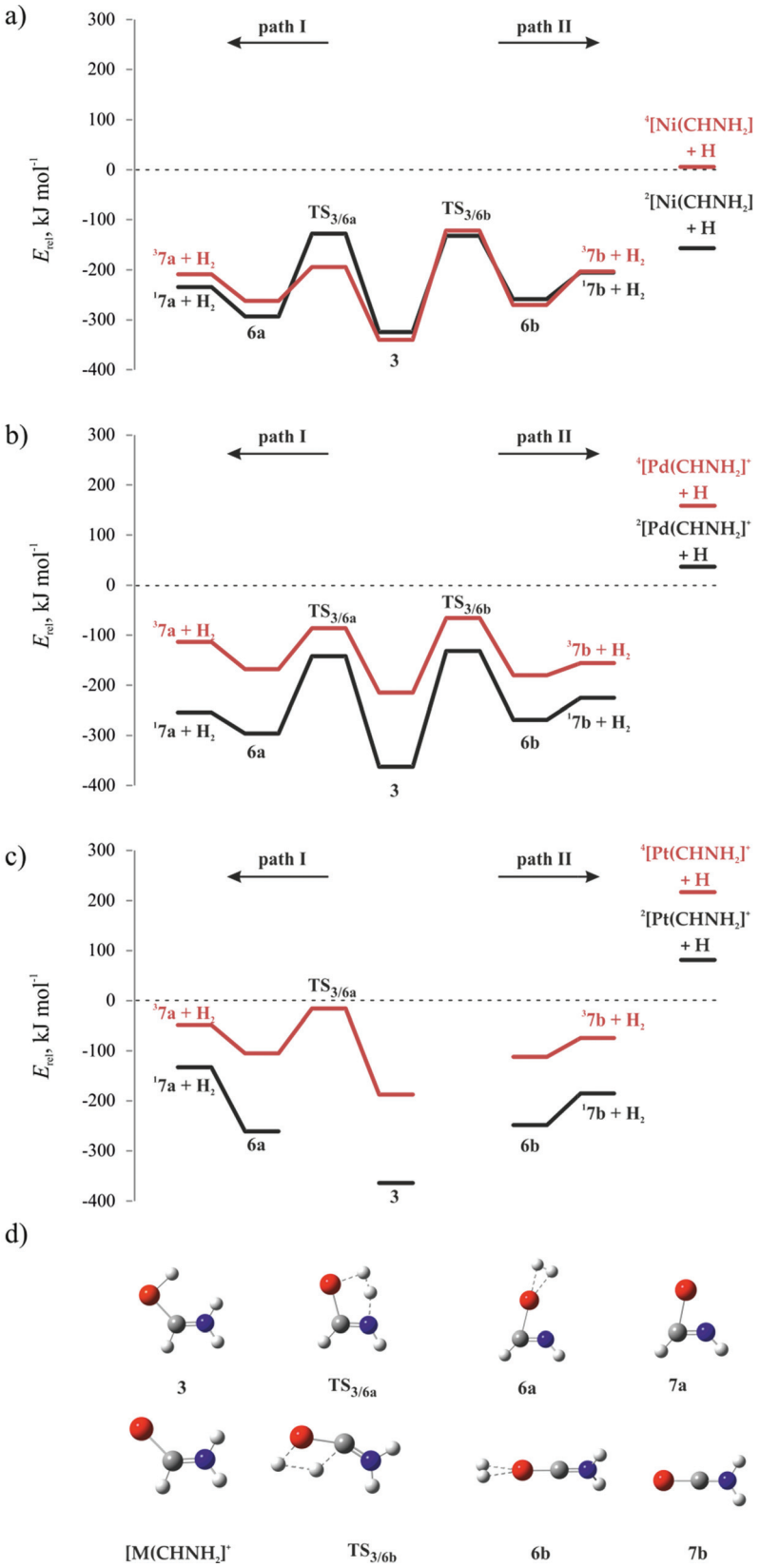

Fig. 3 Schematic potential-energy surfaces for the formations of $[M(CHNH_2)]^+$, $[M(CHNH)]^+$ (**7a**, path I), and $[M(CNH_2)]^+$ (**7b**, path II), respectively, for (a) nickel, (b) palladium, and (c) platinum. The structures of the corresponding minima and transition states are given in (d). The energies are given relative to the singlet ground states of the educts (Fig. 2); for details, also see Table 2. For the sake of clarity, charges are omitted. C ●, H ●, N ●, metal ●.

Table 2 Relative energies (given in kJ mol^{-1}) of all ground (singlet) and first-excited (triplet) state species shown in Fig. 3

	Ni		Pd		Pt	
	s	t	s	t	s	t
$[M(CH)]^+ + NH_3$	0.0	14.9	0.0	53.1	0.0	162.3
3	−324.4	−339.9	−362.7	−214.8	−363.8	−187.6
$[M(CHNH_2)]^+ + H$	−156.1	6.3	37.3	158.4	81.2	216.9
$TS_{3/6a}$	−127.5	−193.9	−141.7	−86.0	[a]	−15.8
6a	−293.2	−262.0	−296.0	−168.1	−261.0	−105.1
$[M(CHNH)]^+ + H_2$	−234.2	−208.7	−254.3	−113.2	−133.0	−48.1
$TS_{3/6b}$	−131.8	−121.4	−131.7	−65.8	[a]	[a]
6b	−258.5	−270.0	−268.8	−179.9	−248.5	−111.8
$[MC(NH_2)]^+ + H_2$	−205.1	−202.9	−224.9	−155.9	−185.2	−74.2

[a] No stable geometry could be obtained.

Table 3 Selected bond lengths (*r*, given in Å) of the singlet species shown in Fig. 2 and 3, the bond lengths of the triplet state species are given in parentheses

	Ni			Pd			Pt		
	r (M–C)	*r* (M–N)	*r* (C–N)	*R* (M–C)	*r* (M–N)	*r* (C–N)	*r* (M–C)	*r* (M–N)	*r* (C–N)
$[M(CH)]^+$	1.61 (1.77)			1.75 (1.85)			1.69 (1.84)		
1	1.61 (1.77)	2.00 (2.00)		1.74 (1.86)	2.18 (2.17)		1.71 (1.80)	2.17 (2.17)	
$TS_{1/2}$	1.61 (1.75)	2.60 (2.35)	2.39 (2.18)	1.77 (1.85)	2.81 (2.55)	2.46 (2.30)	1.70 (1.79)	2.92 (2.70)	2.87 (2.40)
2	1.70 (1.85)		1.52 (1.50)	1.86 (1.96)		1.52 (1.50)	1.79 (1.91)		1.52 (1.50)
$TS_{2/3}$	1.73		1.43	1.90 (1.95)		1.42 (1.42)	1.83 (1.94)		1.44 (1.43)
3	1.80 (2.01)		1.29 (1.29)	1.93 (2.06)		1.29 (1.29)	1.90 (2.02)		1.29 (1.29)
$TS_{3/4}$	1.78 (1.87)		1.31 (1.32)	1.95 (2.05)		1.30 (1.31)	2.00 (2.01)		1.33 (1.32)
$TS_{2/4}$	1.87 (1.87)		1.47 (1.48)	(1.98)		(1.47)	(1.92)		(1.48)
4	1.87 (1.98)		1.41 (1.37)	2.04 (2.25)		1.37 (1.35)	2.03 (2.12)		1.41 (1.37)
$TS_{3/6a}$	1.85 (1.98)		1.25 (1.25)	1.94 (2.13)		1.26 (1.24)	(2.05)		(1.24)
6a	1.85 (1.92)	1.83 (2.06)	1.23 (1.24)	1.98 (2.15)	2.12 (3.00)	1.21 (1.22)	1.95 (2.02)	2.10 (2.83)	1.22 (1.22)
$[M(CHNH)]^+$	1.82 (1.90)	1.83 (2.14)	1.23 (1.24)	1.95 (2.12)	2.20 (2.81)	1.20 (1.21)	1.95 (2.05)	2.06 (2.74)	1.22 (1.21)
$TS_{3/6b}$	1.75 (1.83)		1.28 (1.27)	1.96 (1.99)		1.28 (1.27)			
6b	1.64 (1.84)		1.27 (1.26)	1.82 (1.97)		1.27 (1.27)	1.77 (1.91)		1.27 (1.27)
$[M(CNH_2)]^+$	1.64 (1.84)		1.27 (1.26)	1.80 (1.94)		1.27 (1.27)	1.73 (1.87)		1.27 (1.27)

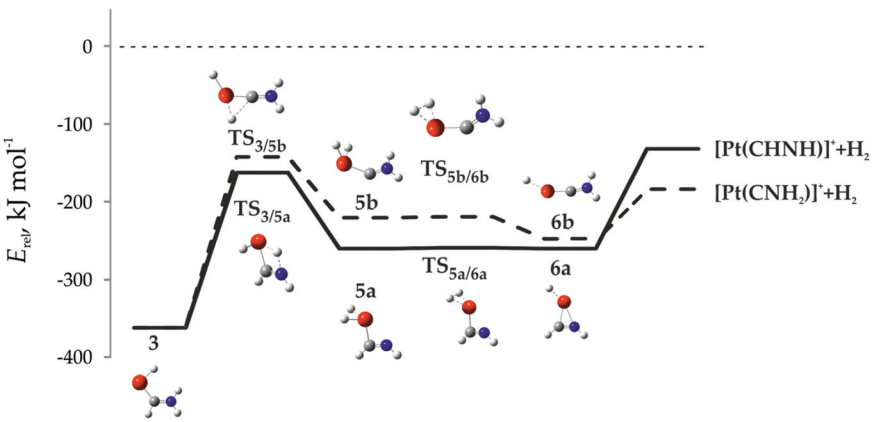

Fig. 4 Schematic potential-energy surfaces for the formations of the two isomers $[^1Pt(CHNH)]^+$ and $[^1Pt(CNH_2)]^+$ by a sequence of oxidative addition and reductive elimination. The energies are given relative to the singlet ground state of the educts $[^1Pt(CH)]^+$ and NH_3 (Fig. 2). For the sake of clarity, charges are omitted. C ●, H ●, N ●, Pt ●.

degenerated reactions of the $[M(CH_3)]^+/CH_4$ pairs (M = Fe, Co, Ni, Ru, Rh, Pd, Os, Ir, Pt).[35] OA/RE scenarios are especially observed in electron-rich, late 4d and 5d transition metal complexes,[36] while the σ-bond metathesis mechanism is typically operative for early transition metals and for those of the first row thus preventing high formal oxidation states.[37] In the present case, the platinum dihydride complexes **5a** and **5b** are formed in a first step, and the subsequent generation of the σ-hydrogen complexes **6a** and **6b** proceeds smoothly and more or less barrier-free (1.0 kJ mol^{-1} and 1.1 kJ mol^{-1} relative

to **5a** and **5b**, respectively). Similar pathways could not be located for nickel and palladium; here, the initial structures converge to the corresponding intermediates shown in Fig. 3 or they are much higher in energy.

Starting from **2**, an alternative reaction path for the formation of $[M(CNH_2)]^+$ is also conceivable, in which the hydrogen of the CH group is transferred in a first step to the metal center and H_2 is formed subsequently from the hydride ligand and one hydrogen of the NH_3 group. While the formation of $[HM(CNH_3)]^+$ is possible from a kinetic as well as thermodynamic point of view, the reaction is kinetically hindered by the barrier associated with the second step, *i.e.* the formation of $[(H_2)M(CNH_2)]^+$; the latter is higher in energy compared to the entrance channel (^{1}Ni: 53.2 kJ mol^{-1}; ^{1}Pd: 28.2 kJ mol^{-1}; ^{1}Pt: 9.9 kJ mol^{-1}).

The data for *r*(M–C) in **3** correspond to the data obtained by the single and the double bond radii approach.[31,32] Depending on the metal, the formations of $[M(CHNH)]^+$ (**7a**, path I) and $[M(CNH_2)]^+$ (**7b**, path II) starting from **3** are associated with different changes in the bond lengths. While the metal-dependent deviations in the M–C bond length in **7a** are more or less minor (0.02 Å–0.05 Å), the values of the M–N bond of this structure are quite different for the Ni, Pd, and Pt systems. For nickel, *r*(Ni–N) = 1.83 Å corresponds to a single bond; in contrast, the values for palladium and platinum (2.20 Å and 2.06 Å) exceed those obtained by the single bond radii approach by 0.18 Å and 0.12 Å, respectively.[31,32] Compared to the formation of **7a**, the changes in the bond lengths accompanied by the formation of $[M(CNH_2)]^+$ (**7b**) are much more pronounced. Starting from **3**, the M–C bond in **7b** is shortened by 0.13 Å to 0.17 Å and also the C–N bond length gets reduced.

With respect to the labeling experiments employing the $[M(CD)]^+/NH_3$ and $[M(CH)]^+/ND_3$ couples, the double N–H bond activation of path I (Fig. 3) results in the loss of H_2 and D_2, respectively, while the C–H and N–H bond formation of path II leads to HD elimination for both isotopologic pairs. However, the losses of H_2 and D_2 from $[M(CD)]^+/NH_3$ and $[M(CH)]^+/ND_3$, respectively, can also be explained by path II if scrambling processes are taken into account, *i.e.* if the system has time enough to pass $\mathbf{TS_{3/6b}}$ back and forth before the elimination of molecular hydrogen occurs; in contrast, the multiple traverse of $\mathbf{TS_{3/6a}}$ does not change the isotopic product pattern. Because $\mathbf{TS_{3/6b}}$ is in the case of nickel energetically more demanding compared to the exit channel, molecular hydrogen is expected to be instantly eliminated after its formation. Based on the calculations, scrambling processes in the $[Ni(CD)]^+/NH_3$ and $[Ni(CH)]^+/ND_3$ pairs can thus be excluded, and the eliminations of H_2/HD and D_2/HD observed in the experiments, respectively, are most likely caused exclusively by the two different reaction pathways of dehydrogenation (Fig. 3). Thus, while $^1\mathbf{TS_{3/6a}}$ and $^1\mathbf{TS_{3/6b}}$ are similar in energy, respectively, $^3\mathbf{TS_{3/6a}}$ is by 72.5 kJ mol^{-1} lower in energy compared to $^3\mathbf{TS_{3/6b}}$, *i.e.* double N–H bond activation according to a TSR scenario is kinetically more favourable, in line with the preferred losses of D_2 and H_2 in the labeling experiments using ND_3 and NH_3, respectively. In contrast, the predominant loss of HD obtained for both the $[Pt(CD)]^+/NH_3$ and $[Pt(CH)]^+/ND_3$ couples points to the preferred formation of $[Pt(CNH_2)]^+$ relative to $[Pt(CHNH)]^+$. Here, the calculated thermochemistry for the formations of both ions agrees with the experimental findings. While $\mathbf{TS_{3/5a}}$ is 20.1 kJ mol^{-1} lower in energy compared to $\mathbf{TS_{3/5b}}$ (Fig. 4), the former transition structure results in the more energy demanding formation of $[Pt(CHNH)]^+$ which is 52.2 kJ mol^{-1} higher in energy compared to $[Pt(CNH_2)]^+$ and 9.2 kJ mol^{-1} higher compared to $\mathbf{TS_{3/5b}}$, respectively; however, both isomers $[Pt(CNH_2)]^+$ and $[Pt(CHNH)]^+$ are accessible under thermal conditions. In the formation of the latter, $\mathbf{TS_{3/5a}}$ is located energetically below the exit channel; however, back reactions to **3** do not affect the isotopic pattern of the product ion and scrambling processes have thus not to be taken into account, indicating that both isomers $[Pt(CNH_2)]^+$ and $[Pt(CHNH)]^+$ are formed in the experiments.

Conclusions

The methylidyne complexes $[M(CH)]^+$ (M = Ni, Pt) have been generated by electrospray ionization (ESI) of solutions of monomeric nickel(II) acetate, $[Ni(CH_3COO)_2]$, and tetrameric platinum(II) acetate, $[Pt_4(CH_3COO)_8]$, in methanol. The so formed ions were allowed to react with ammonia, yielding common as well as different product pairs: while the $M/[CH_2NH_2]^+$ and $[M,C,H_2,N]^+/H_2$ couples are observed for both nickel and platinum, $[M,C,H_3,N]^+/H$ is exclusively formed with M = Ni; in contrast, proton transfer leading to $M/[NH_4]^+$ occurs only for platinum. Regarding the computational investigations, different reaction pathways are involved in the formation of $[CH_2NH_2]^+$ which is accomplished either by a metal-mediated or intra-ligand hydrogen shift. The product ion of H elimination corresponds to $[M(CHNH_2)]^+$; the fact that this complex can only be observed for nickel is a result of an increasing M–H bond strength in the intermediate $[HM(CHNH_2)]$ which leads also to $[M(CHNH)]^+$ and $[M(CNH_2)]^+$. The formations of the latter product ions proceed again *via* different reaction pathways; while for nickel and palladium a σ-bond metathesis is operative, for platinum a sequence of oxidative addition and reductive elimination is involved thus demonstrating metal-depending reaction mechanisms for the same type of reaction.

Acknowledgements

This work is dedicated to Professor Rainer Beckert on the occasion of his 60th birthday. Financial support by the *Fonds der Chemischen Industrie* and the Cluster of Excellence "Unifying Concepts in Catalysis" (EXC 314/1) funded by the *Deutsche Forschungsgemeinschaft* and administered by the Technische Universität Berlin is gratefully acknowledged. We appreciate helpful discussions with Dr. Burkhard Butschke and thank the North-German Supercomputing Alliance (HLRN) for allocating

computer time. R.K. acknowledges the *Stiftung Stipendien-Fonds des Verbandes der Chemischen Industrie* for a Kékulé scholarship and the *Alexander von Humboldt Stiftung* for a Feodor Lynen Research Fellowship.

Notes and references

1 (*a*) A. Deiters and S. F. Martin, *Chem. Rev.*, 2004, **104**, 2199–2238; (*b*) J. P. Corbet and G. Mignani, *Chem. Rev.*, 2006, **106**, 2651–2710; (*c*) R. Hili and A. K. Yudin, *Nat. Chem. Biol.*, 2006, **2**, 284–287; (*d*) M. Kienle, S. R. Dubbaka, K. Brade and P. Knochel, *Eur. J. Org. Chem.*, 2007, 4166–4176; (*e*) F. Monnier and M. Taillefer, *Angew. Chem., Int. Ed.*, 2008, **47**, 3096–3099; (*f*) G. Evano, N. Blanchard and M. Toumi, *Chem. Rev.*, 2008, **108**, 3054–3131; (*g*) F. Monnier and M. Taillefer, *Angew. Chem., Int. Ed.*, 2009, **48**, 6954–6971.

2 (*a*) J. I. van der Vlugt, *Chem. Soc. Rev.*, 2010, **39**, 2302–2322; (*b*) J. L. Klinkenberg and J. F. Hartwig, *Angew. Chem., Int. Ed.*, 2011, **50**, 86–95.

3 (*a*) K. Eller and H. Schwarz, *Chem. Rev.*, 1991, **91**, 1121–1177; (*b*) D. K. Böhme and H. Schwarz, *Angew. Chem., Int. Ed.*, 2005, **44**, 2336–2354; (*c*) J. Roithová and D. Schröder, *Chem. Rev.*, 2010, **110**, 1170–1211; (*d*) D. Agrawal and D. Schröder, *Organometallics*, 2011, **30**, 32–35; (*e*) H. Schwarz, *Angew. Chem., Int. Ed.*, 2011, **50**, 10096–10115; (*f*) D. Schröder, *Acc. Chem. Res.*, 2012, **45**, 1521–1532.

4 (*a*) M. Diefenbach, M. Brönstrup, M. Aschi, D. Schröder and H. Schwarz, *J. Am. Chem. Soc.*, 1999, **121**, 10614–10625; (*b*) K. Koszinowski, D. Schröder and H. Schwarz, *J. Am. Chem. Soc.*, 2003, **125**, 3676–3677; (*c*) K. Koszinowski, D. Schröder and H. Schwarz, *Organometallics*, 2004, **23**, 1132–1139.

5 R. Horn, G. Mestl, M. Thiede, F. C. Jentoft, P. M. Schmidt, M. Bewersdorf, R. Weber and R. Schlögl, *Phys. Chem. Chem. Phys.*, 2004, **6**, 4514–4521.

6 (*a*) M. Aschi, M. Brönstrup, M. Diefenbach, J. N. Harvey, D. Schröder and H. Schwarz, *Angew. Chem., Int. Ed.*, 1998, **37**, 829–832; (*b*) K. Koszinowski, D. Schröder and H. Schwarz, *Organometallics*, 2003, **22**, 3809–3819.

7 B. Butschke and H. Schwarz, *Chem.–Eur. J.*, 2011, **17**, 11761–11772.

8 (*a*) S. W. Buckner, J. R. Gord and B. S. Freiser, *J. Am. Chem. Soc.*, 1988, **110**, 6606–6612; (*b*) D. F. A. Ranatunga, Y. D. Hill and B. S. Freiser, *Organometallics*, 1996, **15**, 1242–1250; (*c*) M. Brönstrup, I. Kretzschmar, D. Schröder and H. Schwarz, *Helv. Chim. Acta*, 1998, **81**, 2348–2369; (*d*) K. Koszinowski, D. Schröder and H. Schwarz, *Angew. Chem., Int. Ed.*, 2004, **43**, 121–124; (*e*) R. Kretschmer, M. Schlangen and H. Schwarz, *Angew. Chem., Int. Ed.*, 2011, **50**, 5387–5391; (*f*) R. Kretschmer, M. Schlangen and H. Schwarz, *Angew. Chem., Int. Ed.*, 2012, **51**, 3483–3488; (*g*) R. Kretschmer, M. Schlangen, M. Kaupp and H. Schwarz, *Organometallics*, 2012, **31**, 3816–3824.

9 (*a*) R. Kretschmer, M. Schlangen and H. Schwarz, *Chem.–Eur. J.*, 2012, **18**, 40–49; (*b*) H. Schwarz and D. Schröder, *Pure Appl. Chem.*, 2000, **72**, 2319–2332.

10 M. Basato, A. Biffis, G. Martinati, C. Tubaro, A. Venzo, P. Ganis and F. Benetollo, *Inorg. Chim. Acta*, 2003, **355**, 399–403.

11 C. Trage, D. Schröder and H. Schwarz, *Chem.–Eur. J.*, 2005, **11**, 619–627.

12 Scientific Instrument Services: Isotope Distribution Calculator and Mass Spec Plotter. http://www.sisweb.com/mstools/isotope.html

13 (*a*) D. Schröder, H. Schwarz, S. Schenk and E. Anders, *Angew. Chem., Int. Ed.*, 2003, **42**, 5087–5090; (*b*) C. Trage, M. Diefenbach, D. Schröder and H. Schwarz, *Chem.–Eur. J.*, 2006, **12**, 2454–2464; (*c*) D. Schröder, M. Engeser, H. Schwarz, E. C. E. Rosenthal, J. Döbler and J. Sauer, *Inorg. Chem.*, 2006, **45**, 6235–6245.

14 M. J. Frisch, G. W. Trucks, H. B. Schlegel, G. E. Scuseria, M. A. Robb, J. R. Cheeseman, G. Scalmani, V. Barone, B. Mennucci, G. A. Petersson, H. Nakatsuji, M. Caricato, X. Li, H. P. Hratchian, A. F. Izmaylov, J. Bloino, G. Zheng, J. L. Sonnenberg, M. Hada, M. Ehara, K. Toyota, R. Fukuda, J. Hasegawa, M. Ishida, T. Nakajima, Y. Honda, O. Kitao, H. Nakai, T. Vreven, J. A. Montgomery, Jr., J. E. Peralta, F. Ogliaro, M. Bearpark, J. J. Heyd, E. Brothers, K. N. Kudin, V. N. Staroverov, R. Kobayashi, J. Normand, K. Raghavachari, A. Rendell, J. C. Burant, S. S. Iyengar, J. Tomasi, M. Cossi, N. Rega, N. J. Millam, M. Klene, J. E. Knox, J. B. Cross, V. Bakken, C. Adamo, J. Jaramillo, R. Gomperts, R. E. Stratmann, O. Yazyev, A. J. Austin, R. Cammi, C. Pomelli, J. W. Ochterski, R. L. Martin, K. Morokuma, V. G. Zakrzewski, G. A. Voth, P. Salvador, J. J. Dannenberg, S. Dapprich, A. D. Daniels, Ö. Farkas, J. B. Foresman, J. V. Ortiz, J. Cioslowski and D. J. Fox, *GAUSSIAN 09 (Revision A.1)*, Gaussian Inc., Wallingford CT, 2009.

15 (*a*) C. Lee, W. Yang and R. G. Parr, *Phys. Rev. B: Condens. Matter*, 1988, **37**, 785–789; (*b*) A. D. Becke, *J. Chem. Phys.*, 1993, **98**, 5648–5652.

16 A. Schäfer, C. Huber and R. Ahlrichs, *J. Chem. Phys.*, 1994, **100**, 5829–5835.

17 (*a*) D. Andrae, U. Häußermann, M. Dolg, H. Stoll and H. Preuss, *Theor. Chim. Acta*, 1990, **77**, 123–141; (*b*) M. Dolg, H. Stoll, H. Preuss and R. M. Pitzer, *J. Chem. Phys.*, 1993, **97**, 5852–5859; (*c*) K. A. Peterson, D. Figgen, M. Dolg and H. Stoll, *J. Chem. Phys.*, 2007, **126**, 124101–124112.

18 X. G. Zhang, R. Liyanage and P. B. Armentrout, *J. Am. Chem. Soc.*, 2001, **123**, 5563–5575.

19 F. Liu, X. G. Zhang and P. B. Armentrout, *Phys. Chem. Chem. Phys.*, 2005, **7**, 1054–1064.

20 K. Levsen and F. W. McLafferty, *J. Am. Chem. Soc.*, 1974, **96**, 139–144.

21 (*a*) K. F. Donchi, B. A. Rumpf, G. D. Willett, J. R. Christie and P. J. Derrick, *J. Am. Chem. Soc.*, 1988, **110**, 347–352; (*b*) S. G. Lias, J. E. Bartmess, J. F. Liebman, J. L. Holmes,

R. D. Levin and W. G. Mallard, *J. Phys. Chem. Ref. Data*, 1988, **17**, 1–861; (*c*) J. M. Dyke, E. P. F. Lee and M. H. Z. Niavaran, *Int. J. Mass Spectrom. Ion Phys.*, 1989, **94**, 221–235; (*d*) E. T. M. Selim, M. A. Rabbih, M. A. Fahmey and M. A. El-Desawy, *Adv. Mass Spectrom.*, 2001, **15**, 779–780.

22 D. Walter and P. B. Armentrout, *J. Am. Chem. Soc.*, 1998, **120**, 3176–3187.

23 Due to relatively low signal-to-noise ratios, the isotopic pattern of the product ions in the dehydrogenation process is associated with rather large error bars; thus, we refrain from modeling the experimental data to a kinetic scheme aimed at specifying the kinetic isotope effects of this reaction.

24 (*a*) J. E. Huheey, E. A. Keiter and R. Steudel, *Anorganische Chemie – Prinzipien von Struktur und Reaktivität*, de Gruyter, Berlin, 4th edn, 2012; (*b*) H. Schwarz, *Angew. Chem., Int. Ed.*, 2003, **42**, 4442–4454.

25 National Institute of Standards and Technology, Chemistry Webbook, http://webbook.nist.gov/chemistry

26 T. Ishikawa, *Jpn. J. Appl. Phys.*, 1993, **32**, 4779–4780.

27 R. L. Kelly, *J. Phys. Chem. Ref. Data*, 1987, **16**, 651–1369.

28 (*a*) P. B. Armentrout, *Annu. Rev. Phys. Chem.*, 1990, **41**, 313–344; (*b*) P. B. Armentrout, *Science*, 1991, **251**, 175–179; (*c*) D. Schröder, S. Shaik and H. Schwarz, *Acc. Chem. Res.*, 2000, **33**, 139–145; (*d*) H. Schwarz, *Int. J. Mass Spectrom.*, 2004, **237**, 75–105.

29 M. Schlangen and H. Schwarz, *J. Catal.*, 2011, **284**, 126–137.

30 P. Pyykkö, S. Riedel and M. Patzschke, *Chem.–Eur. J.*, 2005, **11**, 3511–3520.

31 P. Pyykkö and M. Atsumi, *Chem.–Eur. J.*, 2009, **15**, 12770–12779.

32 P. Pyykkö and M. Atsumi, *Chem.–Eur. J.*, 2009, **15**, 186–197.

33 Q. Zhang and M. T. Bowers, *J. Phys. Chem. A*, 2004, **108**, 9755–9761.

34 M. Schlangen and H. Schwarz, *Angew. Chem., Int. Ed.*, 2007, **46**, 5614–5617.

35 M. Armélin, M. Schlangen and H. Schwarz, *Chem.–Eur. J.*, 2008, **14**, 5229–5236.

36 (*a*) C. Hall and R. N. Perutz, *Chem. Rev.*, 1996, **96**, 3125–3146; (*b*) R. H. Crabtree, *The Organometallic Chemistry of the Transition Metals*, Wiley & Sons, Hoboken, NJ, 5th edn, 2009.

37 (*a*) A. A. Vitale and J. S. Filippo, *J. Am. Chem. Soc.*, 1982, **104**, 7341–7343; (*b*) M. L. Steigerwald and W. A. Goddard Iii, *J. Am. Chem. Soc.*, 1984, **106**, 308–311; (*c*) M. E. Thompson, S. M. Baxter, A. R. Bulls, B. J. Burger, M. C. Nolan, B. D. Santarsiero, W. P. Schaefer and J. E. Bercaw, *J. Am. Chem. Soc.*, 1987, **109**, 203–219.

